Resonant x-ray diffraction of the magnetoresistant perovskite $Pr_{0.6}Ca_{0.4}MnO_3$

S. Grenier,[1,2] J. P. Hill,[2] Doon Gibbs,[2] K. J. Thomas,[2] M. v. Zimmermann,[3] C. S. Nelson,[4] V. Kiryukhin,[1] Y. Tokura,[5] Y. Tomioka,[5] D. Casa,[6] T. Gog,[6] and C. Venkataraman[6]

[1]*Department of Physics and Astronomy, Rutgers University, Piscataway, New Jersey 08854, USA*

[2]*Department of Physics, Brookhaven National Laboratory, Upton, New York 11973, USA*

[3]*Hamburger Synchrotronstrahlungslabor (HASYLAB) at Deutsches Elektronen-Synchrotron (DESY), Notkestrasse 85, 22603 Hamburg, Germany*

[4]*NRL-SRC, NSLS, Brookhaven National Laboratory, Upton, New York, 11973, USA*

[5]*Joint Research Center for Atom Technology (JRCAT), Tsukuba 305-0046, Japan*

[6]*CMC-CAT, Advanced Photon Source, Argonne National Laboratory, Argonne, Illinois 60439, USA*

(Received 8 May 2003; revised manuscript received 21 October 2003; published 15 April 2004)

We report a resonant x-ray-diffraction study of the magnetoresistant perovskite $Pr_{0.6}Ca_{0.4}MnO_3$. We discuss the spectra measured above and below the semiconductor-insulator transition temperature with the aid of a detailed formal analysis of the energy and polarization dependences of the structure factors and *ab initio* calculations of the spectra. In the low-temperature insulating phase, we find that inequivalent Mn atoms order in a CE-type pattern and that the crystallographic structure of $La_{0.5}Ca_{0.5}MnO_3$ [Radaelli *et al.*, Phys. Rev. B **55**, 3015 (1997)] can also describe this system in detail. Instead, the alternative structure proposed for the so-called Zener-polaron model [Daoud-Aladine *et al.*, Phys. Rev. Lett. **89**, 097205 (2002)] is ruled out by crystallographic and spectroscopic evidence. Our analysis *supports* a model involving orbital ordering. However, we confirm that there is no direct evidence of charge disproportionation in the Mn *K*-edge resonant spectra. Therefore, we consider a CE-type model in which there are two Mn sublattices, each with partial e_g occupancy. One sublattice consists of Mn atoms with the $3x^2-r^2$ or $3y^2-r^2$ orbitals partially occupied in an alternating pattern, the other sublattice with the x^2-y^2 orbital partially occupied.

DOI: 10.1103/PhysRevB.69.134419 PACS number(s): 75.47.Lx, 75.47.Gk, 61.10.Nz, 61.10.Ht

I. INTRODUCTION

The interplay among the various electronic degrees of freedom, including those of spin, charge, lattice, and orbital degeneracy, lies at the heart of the wide variety of phenomena observed in strongly correlated electron materials. These include unusual transport properties observed in colossal magnetoresistive (CMR) manganites and high-temperature superconductivity in cuprates. Particularly noteworthy examples of this interplay occur in the perovskite manganites $RE_xAE_{1-x}MnO_3$ (where RE is a trivalent rare earth and AE a divalent alkaline earth) for which the Mn atoms have a partially filled, high-spin, $3d$ band. These materials exhibit rich phase diagrams in which the balance between the various degrees of freedom may be altered by a variety of methods, including hole doping, cationic size mismatch, temperature, pressure, magnetic field and electromagnetic radiation.[1,2]

One of the most interesting ground states that occurs in these phase diagrams arises in the vicinity of half doping ($x=0.5$). This is a phase which has been believed to exhibit charge, orbital, and magnetic order. It is exhibited in a number of compounds, including amongst others $Pr_xCa_{1-x}MnO_3$,[3] $La_xCa_{1-x}MnO_3$,[4,5] and $Nd_{0.5}Sr_{0.5}MnO_3$ (Ref. 6) as well as some other layered manganites such as $La_{1.5}Sr_{0.5}MnO_4$.[7] Further, closely related phases have been observed in cobaltates, e.g., $La_{1.5}Sr_{0.5}CoO_4$ (Ref. 8) and nickelates, e.g., $La_{1.5}Sr_{0.5}NiO_4$.[9] In addition to its ubiquity, it is interesting as an example of the balance among the various degrees of freedom and because in manganites it exhibits the CMR effect: It is an antiferromagnetic insulating phase, but application of a magnetic field melts the charge and orbital order (COO), driving the formation of a ferromagnetic metallic state and thus causing a dramatic decrease in the resistivity. Recent theories suggest that this phenomenon is driven by a competition between charge ordered phases—such as the CE type—and ferromagnetic metallic regions in a phase-separation-type picture.[10]

The search for a microscopic picture of the ground state in half-doped manganites remains a very active field. In the 1950s, Goodenough described the ordering as comprising a checkerboard pattern of Mn^{3+} and Mn^{4+} sites (charge order).[11] In this picture, the Mn^{3+} sites have an extra e_g electron that occupies a $(3z^2-r^2)$-type orbital and these orientationally align in a cooperative manner to form an antiferro-type pattern within the plane (orbital order). On the basis of the exchange pathways set up by this order, a complex magnetic ordering occurs which may be thought of as zigzag chains of ferromagnetically aligned spins which are coupled antiferromagnetically with their neighbors (CE-type antiferromagnetic order). A schematic of this ordering is shown in Fig. 1.

While debate continues as to the origin of the stability of this phase, this original picture has survived relatively unchallenged to the present day, garnering significant theoretical and experimental support. Experimentally, strong evidence includes the various structural studies (both x ray and neutron) which reveal the presence of inequivalent Mn sites, one of which sits in a distorted octahedron consistent with $3z^2-r^2$ occupancy, the other in an undistorted octahedron (see, e.g., Ref. 5). Further, neutron refinements of magnetic moments find two different moments on the two sites, with

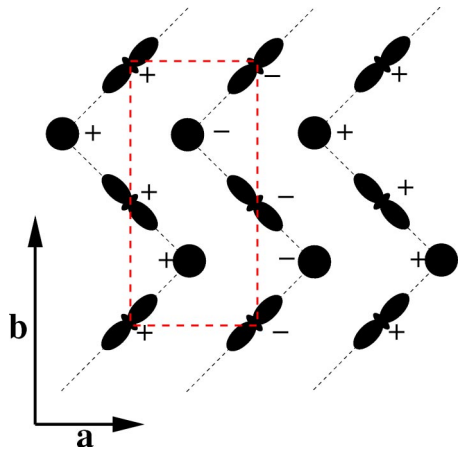

FIG. 1. Schematic of the CE-type charge, orbital, and magnetic ordering as described by Goodenough in 1955 (Ref. 11). The elongated figure-eights represent the occupied e_g $(3x^2-r^2)$-type orbitals on the Mn^{3+} sites, the closed circles represent the Mn^{4+} sites. The signs + and − indicate the relative orientations of the spin. The ferromagnetic zigzag chains are indicated by the dotted lines, the rectangle indicates the low-temperature unit cell.

$\mu(3+)/\mu(4+)\sim 1.1-1.2$ [for instance in $Nd_{0.5}Sr_{0.5}MnO_3$,[12] $La_{0.5}Ca_{0.5}MnO_3$,[5] $La_{0.5}Sr_{1.5}MnO_4$,[7] and $Pr_{0.6}Ca_{0.4}MnO_3$ (Ref. 3)]. In addition, the observed magnetic structure is consistent with expectations for this charge and orbitally ordered structure based on the so-called Goodenough-Kanamori-Anderson rules.[13] Further consistency is found with recent resonant x-ray scattering results which identified short-range orbital correlations as the origin of the observed short-range magnetic correlations on the Mn^{3+} sublattice.[5,14] Finally, transport, optical, and NMR data have all been interpreted in terms of this picture.[1]

Concerning the theory, several groups have argued as to the dominant mechanism leading to the stability of the CE-type phase, but the basic picture has not been questioned.[15–19] However, *ab initio* calculations predict a noninteger mixed valence accompanying an orbitally ordered CE-type phase in half-doped manganites. For $Pr_{0.5}Ca_{0.5}MnO_3$, Anisimov *et al.*[15] showed that two different Mn e_g configurations exist which have almost the same charge density with different orbital configurations. The COO is predicted to be of the checkerboard type, one site having a $(3x^2-r^2)$-type symmetry, the other a (x^2-y^2)-type symmetry. Using the local-spin-density approximation and including the intra-*d*-shell Coulomb interaction, the calculation was performed without the *a priori* constraint of the CE-type pattern and the concomittant Jahn-Teller distortions. A similar description based on density-functional theory using the gradient approximation has also recently been presented for half doped $La_{0.5}Ca_{0.5}MnO_3$.[19] In addition Brink *et al.*[16] proposed that partial charge ordering occurs due to the strong Coulomb repulsion on one site with partly occupied x^2-y^2 and $3z^2-r^2$ orbitals, whereas the adjacent site is occupied either by the $3x^2-r^2$ or $3y^2-r^2$ orbitals.

Despite this body of evidence and the consistency of the COO picture, the nature, the pattern, and even the existence of the Mn valence organization have been recently questioned. In particular, a complete valence separation (i.e., Mn^{3+}/Mn^{4+}) appears to be inconsistent with high-resolution x-ray-absorption near-edge structure (XANES) spectra.[20] Manganites with and without COO show similar XANES spectra which cannot be made up of the sum of the spectra from the parent compounds that have integer valence of 3 + or 4+. These studies suggest that no, or only a small charge disproportionation, either on the manganese atoms or at a molecular scale, can be supported.[20] More explicit is the recent crystallographic structure refinement of Daoud-Aladine *et al.*[21] which was performed without the *a priori* constraints of the mixed-valence pattern: the resulting structure is inconsistent with the CE-type model; it exhibits no significant charge disproportionation and serves as a basis for introducing a model based on so-called Zener polarons. Finally, the resonant x-ray scattering data have been criticized on the grounds that they are mostly sensitive to the position of the oxygen atoms and that it is possible that a purely structural distortion could result in the same scattering patterns.[22] Thus, despite 50 years of experimental and theoretical effort, there remain some very basic questions that remain to be answered in the half-doped manganites.

In this paper, we seek to address this issue by performing resonant x-ray-diffraction (RXD) studies of $Pr_{0.6}Ca_{0.4}MnO_3$, which is believed to exhibit CE-type charge and orbital order. As discussed below, this technique, when accompanied by detailed analysis, is extremely sensitive to the environment of the resonant ion (in this case Mn) and thus the details of the electronic ordering. In particular we analyze the RXD spectra from both above and below the structural phase transition. Our main result from the low-temperature studies is that inequivalent Mn atoms do in fact order in the CE-type pattern. We argue that on one of the sites ("3+") there is indeed $(3x^2-r^2/3y^2-r^2)$-type ordering of the $3d$ e_g orbitals. However, we find no evidence for a chemical shift of the $1s$ levels and interpret this as an absence of significant charge disproportionation. Therefore on the basis of our data, we suggest that the partial occupancy on the "4+" site is in the (x^2-y^2)-type orbital. Finally, all our experimental observations rule out the crystallographic structure upon which the Zener-polaron model was based. They are, however, consistent with the XANES studies.

In Sec. II, we provide details of the sample and the resonant x-ray experiments. In Sec. III, the spectra measured at room temperature ($T>T_{COO}$) and in the low temperature phase ($T_{COO}>T>T_N$) are presented. The results are discussed in Sec. IV and analyzed with the aid of *ab initio* calculations. We summarize our results in Sec. V.

II. MATERIAL AND EXPERIMENTAL METHODS

At room temperature $Pr_{0.6}Ca_{0.4}MnO_3$ has the $Pbnm$ structure[3] (see Fig. 2). At low temperatures, Jirák *et al.*[3] find that the ground state is a CE-type antiferromagnet ($T_N \approx 170$ K), exhibiting charge and orbital order ($T_{COO} \approx 232$ K). The magnetic structure consists of ferromagnetic Mn zigzag chains coupled antiferromagnetically in the (**a**,**b**) plane and stacked ferromagnetically along the **c** direction.

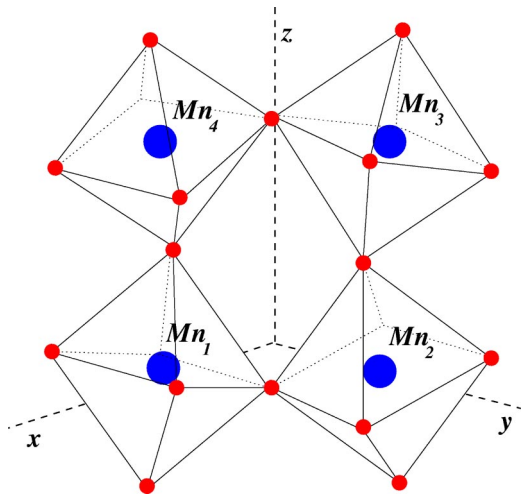

FIG. 2. High-temperature unit cell in the *Pbnm* perovskite structure of $Pr_{0.6}Ca_{0.4}MnO_3$. The oxygen octahedra are all equivalent; Mn_2, Mn_3, and Mn_4 are related to Mn_1 by the *b*, *n*, and *m* mirrors, respectively. Pr/Ca atoms (not shown) lie between the octahedra layers.

The COO phase in $Pr_{0.6}Ca_{0.4}MnO_3$ is evidenced by a sudden decrease in the magnetic susceptibility, an increase in the resistivity at $T_{COO} > T_N$,[23,24] and by the appearance of superstructure Bragg reflections which indicate a doubling of the unit cell. These reflections also disappear when the magnetic field drives the compound into the metallic state.[14] X-ray studies of the superlattice reflections above the transition suggest that charge ordering drives the orbital ordering.[14]

We have chosen the $Pr_{1-x}Ca_xMnO_3$ system for a number of reasons: (i) CMR is observed in a commensurate COO phase which is stabilized for a range of doping $0.3 < x < 0.7$;[23,25] (ii) the similar size of the Ca and Pr cations reduces strain effects; (iii) a further study of the electronic and magnetic phase transitions in this material is advantageous because of the significant difference between the magnetic ordering and COO transition temperatures.

The sample was prepared at the Joint Research Center for Atom Technology in Japan; the growth and the basic transport properties have been described in detail elsewhere.[23] The (010) surface was polished with a 1 μm grit and the mosaic of the sample was 0.25° full width at half maximum as measured at the (020) reflection.

The experiments were performed utilizing resonant x-ray diffraction which involve measuring the intensity of a reflection as a function of the incident photon energy.[26–30] By tuning the incident energy to the Mn absorption *K* edge, 1*s* electrons are promoted to an intermediate unoccupied *p* state and then decay back to the 1*s*. Therefore one probes the unoccupied density of *p* states projected onto the Mn atoms as a function of energy. Because these intermediate states reflect any structural anisotropy, the scattering factors of the Mn atoms are no longer scalars but become tensors. In addition, the coherence of the resonant process implies that diffraction can occur and we can probe the long-range-ordered correlations of the local electronic configuration: This technique combines spectroscopic information with that of a scattering experiment.

The Mn 4*p* states are sensitive to the surrounding structure because their spatial distribution extends out to, and beyond, the Mn nearest neighbors. In order to interpret the RXD spectra measured at the *K* edge, we therefore make the assumption that the particular structural distortions of the Mn surroundings reflect the highest occupied 3*d* orbitals. We note that the characteristic time for the resonant process is about 10^{-16} s while that of the lattice vibrations is 10^{-12} s and therefore RXD provides a snapshot of the distortions surrounding the Mn atoms.

Interpreting these particular resonant spectra is still complex. According to previous works in the literature, it is not possible to draw conclusions about the surrounding structure, or the charge or orbital ordering without detailed, quantitative modeling and analysis of the various contributions to the resonant scattering. Below, we provide a description of the resonant structure factor within the dipolar approximation, both above and below the phase-transition temperature. These calculations provide an understanding of the characteristics of the resonant signals which allow us to infer the characteristics of the electronic configuration. In particular, we are interested in determining the symmetries of the highest occupied orbitals.

The x-ray experiments were performed at the CMC-CAT undulator beamline 9IDB at the Advanced Photon Source (Argonne National Laboratory) and at beamline X22C at the National Synchrotron Light Source (Brookhaven National Laboratory). Beamline 9IDB possesses a double-crystal Si (111) monochromator with an energy resolution of $\Delta E/E \approx 2 \times 10^{-4}$. Beamline X22C has a double Ge (111) monochromator with a resolution $\Delta E/E \approx 5 \times 10^{-4}$. We have focused on the incident energy dependence of the diffracted intensity, as it is tuned through the Pr-L_{II} and Mn-*K* absorption edges which in this oxide are at 6444 eV and 6552 eV, respectively, where we have defined the position of the edge by the maximum of the first derivative of the absorption spectrum. In this paper we focus on the vicinity of the Mn *K*-edge energy. For some of the data collected, the scattering was resolved into the respective σ-σ' and σ-π' polarization channels, where we adopt the standard notation that σ (π) denotes the polarization perpendicular (parallel) to the scattering plane (see Fig. 3). The polarization analysis was performed by utilizing a Cu (220) analyzer crystal for which $2\theta_{Bragg} \approx 96°$ at the Mn *K* edge. This discrepancy from the ideal 90° leads to an expected leakage of about $\cos^2(96) \approx 1.1\%$ for the projection of one polarization component into the other one. By measuring the fully σ-σ' polarized Bragg reflection (020) in the σ-π' channel analyzer we measured the leakage to be about 1.5%. High-**Q** resolution measurements were performed with a Ge(111) analyzer crystal. In addition to the diffraction experiment, complementary XANES measurements were performed on the same sample. These two techniques probe the same resonant scattering factors; though the XANES measurement lacks the site selectivity of resonant diffraction, it provides the average of the imaginary part of the resonant scattering factor directly. These latter measurements were carried out at room temperature at beamline X11A (National Synchrotron Light Source, Brookhaven National Laboratory). This beamline has a

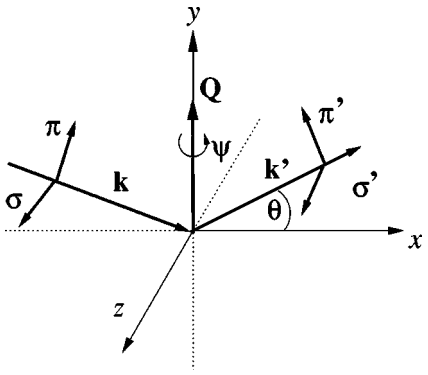

FIG. 3. The diffraction geometry. An azimuthal scan consists of rotating the sample by an angle ψ around the diffraction vector $\mathbf{Q}=\mathbf{k}'-\mathbf{k}$. The vectors σ and π are the basis for the polarization vector of the photon.

double-crystal Si (111) monochromator. The 6.539 keV *K* edge of a Mn foil was used to calibrate the energy at all beamlines.

III. EXPERIMENTAL RESULTS

A. High-temperature phase ($T>T_{COO}$)

RXD spectra were collected in the high-temperature phase in order to provide a base line to compare to the low-temperature ordered phase. Figure 4 shows the RXD spectrum of the forbidden (010) reflection in the σ-π' channel taken over a wide energy range at 280 K, i.e., well above the phase transition. It has no σ-σ' component. The XANES spectrum at room temperature is also shown on the same energy scale.

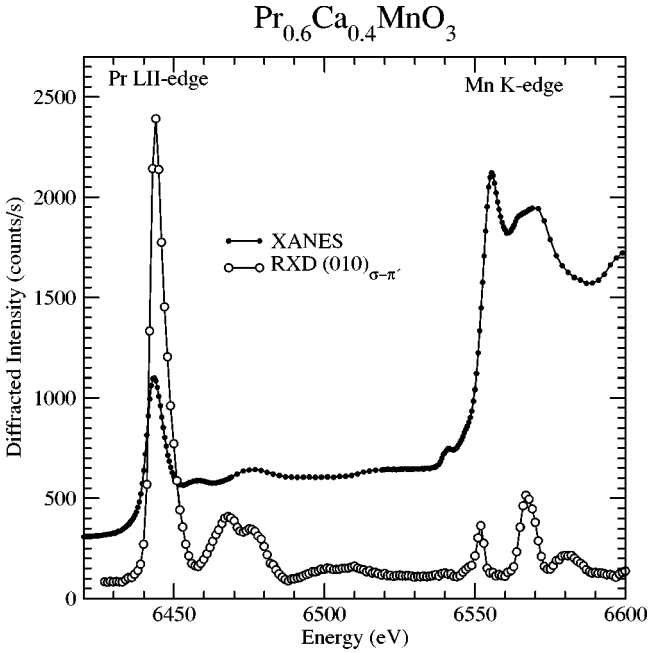

FIG. 4. (Open circles) Resonant x-ray diffraction (RXD) of the $(010)_{\sigma-\pi'}$ *Pbnm*-forbidden peak measured in the σ-π' channel at 280 K ($T>T_{COO}$) through the Pr L_{II} edge (6444 eV) and the Mn *K* edge (6552 eV). The incident polarization is directed along the **a** axis, i.e., $\psi=90°$. The room-temperature x-ray-absorption near-edge structure (XANES) spectra (closed circles) are also shown over the same energy interval.

A number of features are seen in the RXD spectrum, prominently at the Pr L_{II} and Mn *K* edges. At the Pr L_{II} edge one observes three peaks, the main peak coinciding with the maximum of the absorption spectra. At the Mn *K* edge, the spectrum shows three peaks each with a Gaussian line shape with half-widths that increase as a function of the energy. In contrast to the Pr L_{II} edge, the first peak at $E_i=6552$ eV coincides with the maximum of the first derivative of the absorption spectrum. As we will discuss below, the origin of this signal is due to the loss of the exact octahedral symmetry around the Mn atoms as a result of the tilt ordering. The $(010)_{\sigma-\pi'}$ reflection has long-range order, that is, its width in reciprocal space, as measured at the Mn *K* edge with a Ge (111) analyzer, is similar to that of the (020) Bragg reflection. Thus, this scattering at (010) is distinct from that of the pretransitional fluctuations just above T_{COO} observed in the σ-σ' channel, which exhibit temperature-dependent short-range order.[14] Rather, this scattering represents the average long-ranged-ordered component of the high-temperature structure (Templeton scattering[31]).

The XANES measurements were performed by measuring the total fluorescence yield with the beam along the [010] direction and with the incident polarization vector along both **a** and **c**. In fact, this rotation of 90° around the incident direction produced no measurable change in the spectral features. It seems likely that the footprint of the beam is sufficient to overlap different *a*, *b*, and *c* domains in this twinned sample such that the resulting XANES spectrum is an average over these domains and thus independent of the nominal polarization direction.

B. Low-temperature phase ($T<T_{COO}$)

In the low-temperature phase, Zimmermann *et al.*[14] reported and discussed the spectra of the (010), (030), $(0\frac{1}{2}0)$, and $(0\frac{5}{2}0)$ reflections, together with their polarization dependence. In Fig. 5, we report data for the energy dependence of the $(010)_{\sigma-\sigma'}$ and $(030)_{\sigma-\sigma'}$. These data were taken with a higher-energy resolution, which is 1.5 eV compared to the earlier 5 eV resolution.[14] The overall shape is the same as the earlier data with no change in the energy widths of the observed features, indicating that they were not resolution limited in the earlier data set. That is, the observed widths are determined by the finite lifetime of the excited electron-hole pair and by band-structure effects.

There is, however, a small difference between these data and the earlier scans, namely the feature observed around 6542 eV in both spectra in Fig. 5. We attribute this to the pre-edge transitions (i.e., $1s\rightarrow 3d$)—possibly dipole allowed from the breaking of inversion symmetry at the Mn site. Such transitions are expected to be relatively sharp and thus would have been smeared out in the earlier, lower-resolution data.

For completeness we reproduce the $(0\frac{3}{2}0)_{\sigma-\pi'}$ RXD of Zimmermann *et al.*[14] in Fig. 6 and show unpublished data of

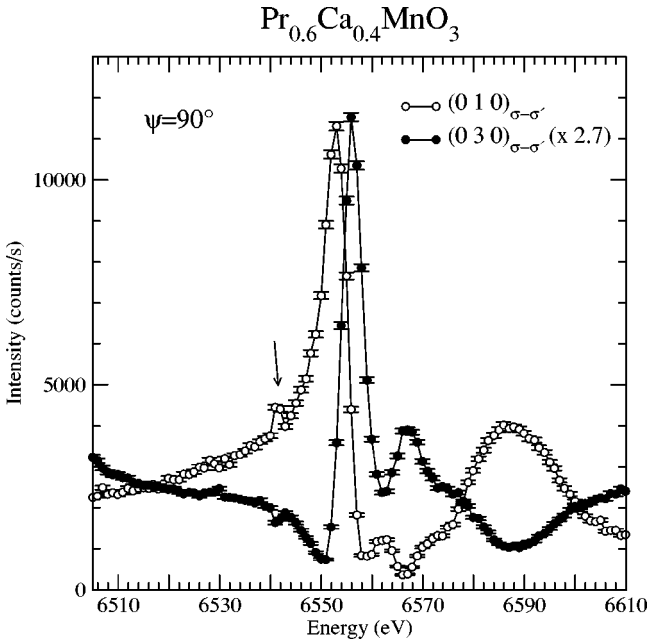

FIG. 5. RXD spectra of the $(010)_{\sigma\text{-}\sigma'}$ and $(030)_{\sigma\text{-}\sigma'}$ reflections at 100 K. The 3 eV difference between the two maxima is due to the different crystallographic structure factors (Ref. 14). The small feature at 6542 eV (arrow) is attributed to the pre-edge transition. This feature was not seen in the previous data (Ref. 14) because of the lower resolution of that data set. The incident polarization is along the **a** axis, i.e., $\psi = 90°$.

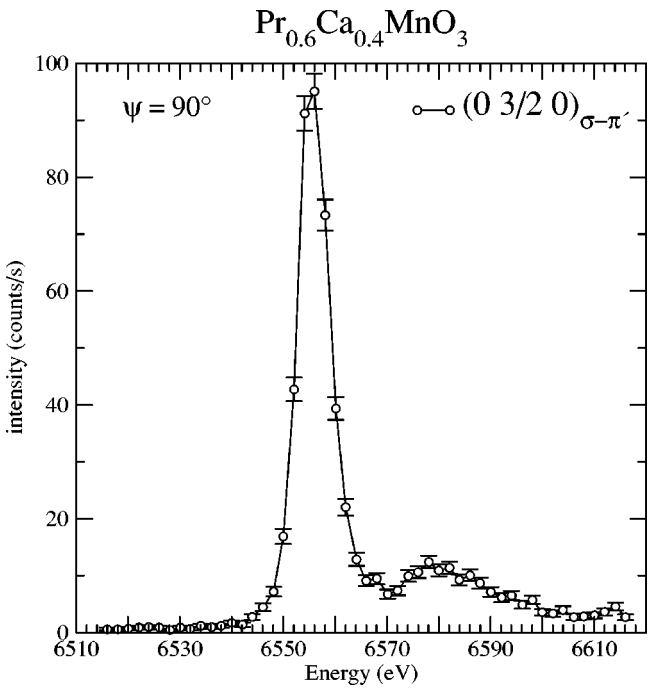

FIG. 6. RXD spectrum of the $(0\frac{3}{2}0)_{\sigma-\pi'}$ reflection at 10 K reproduced from (Ref. 14). The energy dependence is strongly reminiscent of the Jahn-Teller compound $LaMnO_3$ which has an orbital ordering of the highest $3d$ orbital occupied (Fig. 7). The energy resolution for these data was about 5 eV.

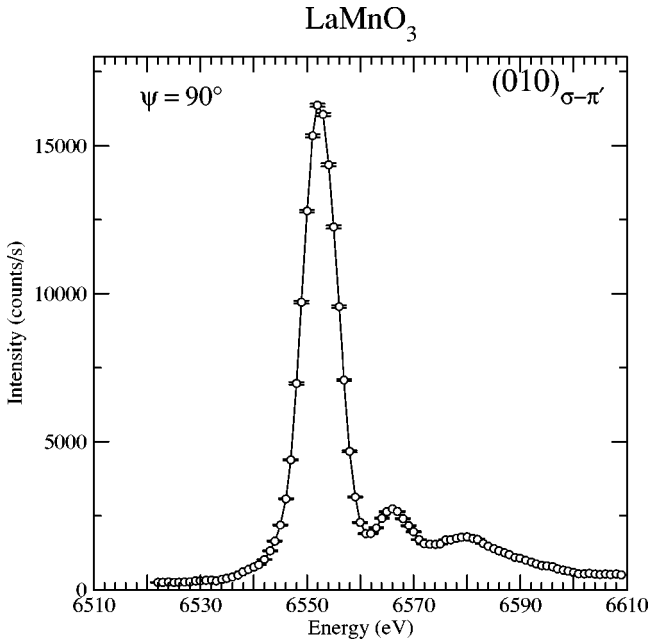

FIG. 7. RXD spectrum of the $(010)_{\sigma\text{-}\pi'}$ of $LaMnO_3$. The strong resonance arises from the Jahn-Teller distortion of the oxygen octahedra due to the orbital ordering (Ref. 27). The energy resolution for these data was about 5 eV.

the $(010)_{\sigma\text{-}\pi'}$ measured on $LaMnO_3$ in the orbital ordered phase in Fig. 7. Note that the orbital order in $LaMnO_3$ has a propagation vector equal to (010), whereas in $Pr_{0.6}Ca_{0.4}MnO_3$ it is equal to $(0\frac{1}{2}0)$.

The spectrum of the $(010)_{\sigma\text{-}\pi'}$ reflection of $Pr_{0.6}Ca_{0.4}MnO_3$ was also measured at low temperature. Unfortunately, at these temperatures, there is significant scattering in the σ-σ' channel at this wave vector and care must be taken that leakage from this channel is not falsely ascribed to σ-π' scattering. The severity of this problem is illustrated in Fig. 8, which shows that the 1.5% leakage of the present analyzer is sufficient to account for almost all of the apparent σ-π' scattering at $T = 180$ K in the first ($E_i = 6552$ eV) and third ($E_i = 6580$ eV) features.

Note that no absorption correction has been made in these spectra. In addition, the spectra were checked to be free of spurious multiple scattering by rotating the sample around the diffraction vector.

IV. DISCUSSION

A. High-temperature phase ($T > T_{COO}$)

Above the phase-transition temperature $T_{COO} = 232$ K, the crystallographic structure is described by the *Pbnm* space group with one Mn atom sitting at four equivalent sites.[3] The structure is orthorhombic, pseudocubic, and the lattice parameters are $a = 5.4315$ Å, $b = 5.446$ Å, and $c = 7.6481$ Å (throughout this paper all crystallographic notations will refer to the *Pbnm* unit cell, even at low temperatures where the space-group symmetry is actually lowered). Figure 2 shows the unit cell with the four Mn sites that are related by the symmetries of the space group *Pbnm.* The Mn are situated in

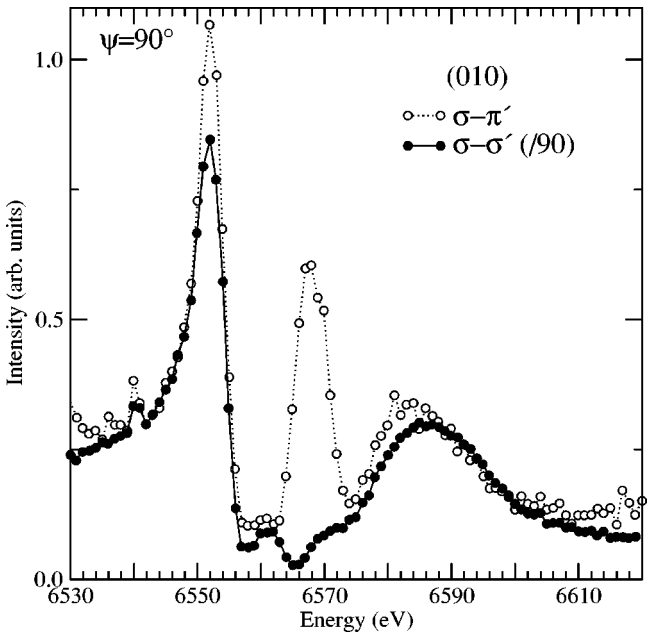

FIG. 8. Measurement of the two scattering channels with the Cu(220) analyzer in the vicinity of the Mn *K* edge at the (010) reflection at 180 K. The figure illustrates the contamination of the σ-π' channel measurement by the σ-σ' channel. The intensity from the σ-σ' channel has been scaled to show that a leakage of about 1% leads to a significant contamination of the σ-π' channel in the ordered phase. This complicates the analysis of the low-temperature phase (see text). However, the second resonance at about 6570 eV is almost uncontaminated.

oxygen octahedra. The structure shows the $GdFeO_3$-type distortion, that is, the octahedra are actually tilted from the **c** axis in the **a** direction.[32,33] They are compressed along the **c** axis (Mn-O_z = 1.9544 Å) and expanded in the (**ab**) plane (Mn-O_{xy} = 1.9738 Å, Mn-O_{xy} = 1.9714 Å).

In the following we derive several resonant structure factors of the Mn atoms. Similar approaches have been taken previously by Murakami *et al.*,[27] Takahashi *et al.*,[34] and García *et al.*[22] These expressions will serve as a comparison with those derived later for the low-temperature phase. In order to quantify the resonant x-ray cross section of this distorted structure one has to take into account the resulting anisotropy of the crystal field around the Mn sites. Within the dipolar approximation ($E1$), the scattering amplitude is then described as a tensor of rank two.[26] In the following *x*, *y*, and *z* are defined along the crystallographic axes (see Fig. 2). By assigning to one of the Mn atoms, Mn_1, the most general dipolar tensor f_1 and then applying the mirror symmetries of the *Pbnm* space group, as represented by the matrices M_x, M_y, and M_z, one can generate the scattering tensors for the four equivalent Mn atoms:

$$f_1 = \begin{pmatrix} f_{xx} & f_{xy} & f_{xz} \\ f_{xy} & f_{yy} & f_{yz} \\ f_{xz} & f_{yz} & f_{zz} \end{pmatrix}, \tag{1}$$

$$f_2 = M_x f_1 M_x = \begin{pmatrix} f_{xx} & -f_{xy} & -f_{xz} \\ -f_{xy} & f_{yy} & f_{yz} \\ -f_{xz} & f_{yz} & f_{zz} \end{pmatrix},$$

$$f_3 = M_y f_1 M_y = \begin{pmatrix} f_{xx} & -f_{xy} & f_{xz} \\ -f_{xy} & f_{yy} & -f_{yz} \\ f_{xz} & -f_{yz} & f_{zz} \end{pmatrix},$$

$$f_4 = M_z f_1 M_z = \begin{pmatrix} f_{xx} & f_{xy} & -f_{xz} \\ f_{xy} & f_{yy} & -f_{yz} \\ -f_{xz} & -f_{yz} & f_{zz} \end{pmatrix}.$$

When the incident energy is tuned to the Mn absorption edge, the scattering power of each of these crystallographically equivalent atoms may be represented by these matrices. One sees that as a result of the symmetry operations, they are not the same. The scattering then becomes polarization dependent and the standard crystallographic reflection conditions are altered.[35] The off-diagonal terms of the scattering tensor give rise to these effects and are nonzero at the absorption edge because the intermediate electronic states are anisotropic. As a result, the Mn sites give an anomalous contribution to the *Pbnm*-forbidden reflections such as $(h00)$, $(0k0)$, or $(0k\ell)$, whereas the contributions of O, Ca, and Pr, which have isotropic scattering factors, cancel exactly. We consider below the total structure factors for the Mn atoms at several forbidden reflections:

$$F^{\mathrm{Mn}}(h00) = F^{\mathrm{Mn}}(0k0) = f_1 - f_2 - f_3 + f_4 = 4f_{xy}\begin{pmatrix} 0 & 1 & 0 \\ 1 & 0 & 0 \\ 0 & 0 & 0 \end{pmatrix},$$

$$F^{\mathrm{Mn}}(00\ell) = f_1 + f_2 - f_3 - f_4 = 4f_{yz}\begin{pmatrix} 0 & 0 & 0 \\ 0 & 0 & 1 \\ 0 & 1 & 0 \end{pmatrix},$$

$$F^{\mathrm{Mn}}(0k\ell) = f_1 - f_2 + f_3 - f_4 = 4f_{xz}\begin{pmatrix} 0 & 0 & 1 \\ 0 & 0 & 0 \\ 1 & 0 & 0 \end{pmatrix}, \tag{2}$$

with *h*, *k* and ℓ being odd. Different energy dependences of the resonant spectra are expected for these reflections since each probes different components of the Mn resonant scattering tensor.

We next use these tensors to calculate the polarization and azimuthal dependences of the intensity within the two common experimental geometries σ-σ' and σ-π' (see Fig. 3). We define the azimuthal angle ψ as the angle between the incident polarization vector σ and the **c** axis, for the $(h00)$ and $(0k0)$ reflections, and the angle between σ and the **a** axis for the (00ℓ) and $(0k\ell)$ reflections. An azimuthal scan of one particular reflection corresponds to measuring the in-

tensity on rotating the sample an angle ψ in the plane perpendicular to the diffraction vector. With these definitions, the polarization vectors are

$$\sigma(h00)=(0,-\sin\psi,\cos\psi),$$

$$\pi'(h00)=(\cos\theta_B,-\sin\theta_B\cos\psi,-\sin\theta_B\sin\psi),$$

$$\sigma(0k0)=(\sin\psi,0,\cos\psi),$$

$$\pi'(0k0)=(-\sin\theta_B\cos\psi,\cos\theta_B,\sin\theta_B\sin\psi),$$

$$\sigma(00\ell)=(\cos\psi,\sin\psi,0),$$

$$\pi'(00\ell)=(\sin\psi\sin\theta_B,-\cos\psi\sin\theta_B,\cos\theta_B),$$

$$\sigma(0k\ell)=(\cos\psi,\sin\psi\cos\alpha,-\sin\psi\sin\alpha),$$

$$\pi'(0k\ell)=(\sin\theta\sin\psi,\ \cos\theta_B\sin\alpha-\sin\theta_B\cos\psi\cos\alpha,$$

$$\sin\theta_B\cos\psi\sin\alpha+\cos\theta_B\cos\alpha), \tag{3}$$

where θ_B is the Bragg angle and $\alpha=\arctan c/b$. Then, for example, the scattering from the $(0k\ell)$ reflection for a σ-π' diffraction geometry is given by $I_{\sigma\text{-}\pi'}(0k\ell)=|\sigma(0k\ell)F(0k\ell)\pi'(0k\ell)|^2$. The intensities corresponding to the above structure factors are

$$I_{\sigma\text{-}\sigma'}(h00)=I_{\sigma\text{-}\sigma'}(0k0)=0, \tag{4}$$

$$I_{\sigma\text{-}\pi'}(h00)=I_{\sigma\text{-}\pi'}(0k0)=|4f_{xy}\cos\theta_B\sin\psi|^2, \tag{5}$$

$$I_{\sigma\text{-}\sigma'}(00\ell)=0, I_{\sigma\text{-}\pi'}(00\ell)=|4f_{yz}\cos\theta_B\sin\psi|^2, \tag{6}$$

$$I_{\sigma\text{-}\sigma'}(0k\ell)=|4f_{xz}\sin2\psi\sin\alpha|^2, \tag{7}$$

$$I_{\sigma\text{-}\pi'}(0k\ell)=|4f_{xz}|^2|(\sin\theta_B\sin\alpha\cos2\psi+\cos\theta_B\cos\alpha\cos\psi)|^2. \tag{8}$$

These calculations show that $I_{\sigma\text{-}\pi'}(0k0)$ and $I_{\sigma\text{-}\pi'}(00\ell)$ have twofold symmetry with respect to ψ and that the σ-σ' channel is non-zero for the forbidden $(0k\ell)$ reflections. $I_{\sigma\text{-}\sigma'}(0k\ell)$ and $I_{\sigma\text{-}\pi'}(0k\ell)$ are proportional to each other as a function of the x-ray energy but differ in their azimuthal symmetries, the σ-σ' channel being fourfold symmetric in ψ while the σ-π' channel has no particular symmetry. All of these characteristics have been observed in perovskite oxides of this space group.[27,36,37] An incident π component can also give a contribution to the π'-polarized scattering. However, considering the highly linearly polarized synchrotron source, the beamline optics and the vertical diffraction geometry we used, the incident π component is expected to be much smaller than the incident σ component and will not be considered in the following [there also systematic extinctions, in particular $F_{\pi-\pi'}(0k0)=0$ at all ψ].

The particular azimuthal dependences arise due to a geometrical effect—a result of the symmetries between the equivalent resonant atoms in the *Pbnm* space group. So, the azimuthal dependence *per se* is independent of the anisotropy in the occupied and unoccupied density of states. Rather a more detailed analysis is required before a conclusion concerning orbital occupancies may be drawn. This calculation of the resonant intensity is widely applicable since the space group *Pbnm* describes many other manganite, titanate, and vanadate perovskites.[34,38,39] Note that this space group includes both compounds that are orbitally ordered and some that are orbitally disordered, as in the present case.

As a result of the tilting of the octahedra relative to the crystallographic axes, nonzero off-diagonal elements are introduced into the scattering tensor. That is, the off-diagonal terms come from both the different lengths of the principal directions of the octahedra (i.e., an asymmetry inside the octahedra), and from the tilt of the octahedra off the crystallographic axes (asymmetry outside the octahedra). One expects that the further the octahedra are tilted from the polarization direction the more important the off-diagonal terms become. Conversely, decreasing the degree of tilt decreases the signal arising from the distortion of the octahedra: If the principal axis of the octahedra were along the crystallographic axes, then $f_{xy}=f_{xz}=f_{yz}=0$, and F^{Mn} would become diagonal and the signal would disappear. In a sense then, the intensity of the whole resonant spectrum is modulated by the degree of octahedral tilt.

From Eq. (4), we see that the experimental measurement of the $(010)_{\sigma\text{-}\pi'}$ reflection at $\psi=90°$ measures $|f_{xy}|$. One notes that for this reflection the resonance at the edge (6552 eV) has a lower intensity than the second resonance at 6568 eV (Fig. 4). Interestingly, this is in contrast with the data for $LaMnO_3$. The two compounds have a similar overall structure in the same space group, but $LaMnO_3$ shows orbital ordering.[40] In $LaMnO_3$, the first resonance for the same reflection $(010)_{\sigma\text{-}\pi'}$ is much larger, and is understood as coming mainly from the in-plane Jahn-Teller distortion that reveals the orbital ordering.[27,28,41] For $LaMnO_3$ the in-plane Mn-O distances are Mn-$O_{xy}=1.907$ Å, Mn-$O_{\bar{xy}}=2.178$ Å.[40] For $Pr_{0.6}Ca_{0.4}MnO_3$, the anisotropy in the plane at room temperature is much smaller. The distances are Mn-$O_{xy}=1.971$ Å, Mn-$O_{\bar{xy}}=1.974$ Å.[3] This lower anisotropy is revealed qualitatively by a much lower intensity of the first resonance. Recently, Takahashi, Igarashi, and Fulde performed *ab initio* calculations for $LaMnO_3$, $YTiO_3$, and YVO_3 in the orbitally ordered phases.[34,38,39] These authors completed calculations of the σ-π' channel without including any ordering of the $3d$ orbitals, thereby emphasizing the role of the structural distortions as an origin of the resonant signal. From this, they inferred that the first peak in the Mn spectra arises mainly from the in-plane anisotropy, and that the second was largely due to the tilt order. Thus, this interpretation of the calculations seems consistent with the data presented in Fig. 4 and those of $LaMnO_3$, given the difference between the in-plane anisotropy in the two cases. In addition, as discussed above, we believe that the tilt also has an effect over the entire spectrum (that is, the influence of the tilt order is not confined to the second peak).

In order to gain further insight into the electronic configuration of the Mn in this doped manganite, we next present preliminary *ab initio* calculations of the resonant diffraction. In particular, we want to investigate whether the known structural distortions are enough to give rise to the resonant

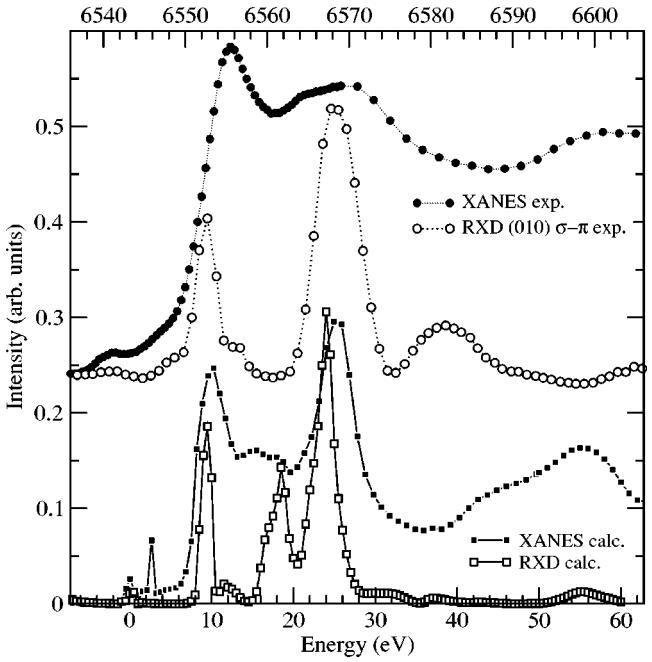

FIG. 9. RXD of the (010) reflection and XANES from an *ab initio* calculation (see text) compared to the experimental spectra taken at room temperature. For the XANES spectra the polarization is averaged both in the calculation and in the measurement.

signal observed in $Pr_{0.6}Ca_{0.4}MnO_3$ above the charge and orbital order temperature. Our calculations of the $(010)_{\sigma\text{-}\pi'}$ have been done in the framework of the full multiple-scattering theory with the FDMNES code.[42] Starting with the atomic positions and their associated electronic densities, this code solves the Green's matrix for the intermediate states to which the photoelectron is promoted. The structure used is that of Jirák *et al.*[3] but with all the RE sites replaced by Ca—the ability to treat a random distribution of Pr and Ca ions is beyond the scope of the present work. In addition, the electronic configurations of the atoms are described as if they were isolated, that is, Mn is $3d^5 4s^2$ and so on. The Hedin-Lundquist exchange-correlation potential is used.

The results of these calculations are shown in Fig. 9, which compares the XANES and the RXD measured at room temperature with the calculations of each. The preliminary results are quite satisfactory despite the simplistic approximations used and the fact that no broadening for the core-hole lifetime or the energy resolution has been applied. The main disagreement is the peak at 18 eV in the calculation of the RXD. These results suggest that no detailed description of the Mn $3d$ orbitals is needed to predict qualitatively the appearance of resonance peaks at high temperature. All that is needed is the anisotropic structural configuration.

B. Low-temperature phase ($T < T_{COO}$)

Below T_{COO}, two sets of peaks appear at (i) $Q+(010)$ and $Q+(100)$, and (ii) at $Q+(0\frac{1}{2}0)$, where Q stands for the diffraction vector of the Bragg reflections allowed in the *Pbnm* space group. The latter superstructure peaks indicate a doubling of the unit cell along the **b** direction. The intensity of these two types of reflections shows the same temperature dependence; however, they are differentiated by their different correlation lengths within the low-temperature phase.[33] In the framework of the COO picture, the $Q+(0\frac{1}{2}0)$ reflections are due to distortions induced by the orbital order. The orbital order forms in a domain state with randomly distributed antiphase boundaries formed by misoriented orbitals. The domains are characterized by a correlation length $\xi = 320 \pm 10$ Å.[5,33] In contrast the $[Q+(010)]$-type reflections are resolution or near-resolution limited with a correlation length $\xi > 2000$ Å.

A strong resonance effect is observed at the superstructure reflections $(0\frac{3}{2}0)_{\sigma\text{-}\pi'}$, $(010)_{\sigma\text{-}\sigma'}$, and $(030)_{\sigma\text{-}\sigma'}$ when the polarization is in the (**ab**) plane ($\psi = 90°$) (Figs. 5 and 6). In particular, the resonant effect at the $Q+(010)$ reflection may be described qualitatively as a "derivative effect,"[6,43] that is, the line shape in the energy scan has the form of the derivative of the resonant factors. This is a clear signal of the presence of one element sitting at two *different* crystallographic sites which contribute to the structure factor with opposite phase.

In the literature, the appearance of the derivative effect has usually been said to be a direct observation of charge ordering.[6,43–45] The argument is that the decrease (increase) of the electronic density of the resonant atom lowers (raises) the energy of the initial $1s$ core level resulting in a tighter (weaker) binding energy. In this picture, this shift applies directly to the x-ray resonant factors of the Mn^{4+} (Mn^{3+}) which shift to higher (lower) energy at the Mn K edge (i.e., for transitions from $1s$ to p states). It is noteworthy that any $1s$ shift has an isotropic effect on the spectra, whereas any shift of the $4p$ will depend on the Mn-O distances and will therefore be anisotropic. The combination of both shifts constitutes the chemical shift. For example, an isotropic shift occurs in the highly anisotropic vanadium site in the charge ordered phase of $\alpha' - NaV_2O_5$ for which the derivative effect has been observed for two perpendicular directions of the incident polarization with the same energy shift.[43] However, in the present compound the resonant signal disappears when the polarization is along the **c** axis ($\psi = 0°$).[14] Thus, the simplest picture of an isotropic chemical shift of only the $1s$ core levels does not apply here. This observation has also been made in other perovskites, including manganites.[6] To understand the resonance behavior in these materials therefore requires a more quantitative study, which we develop in the following.

1. Low-temperature structure factor

In the doubled low-temperature unit cell there are eight Mn atoms. As widely observed in the three-dimensional manganites,[5,21,46] the planes are believed to be equivalent along the **c** axis, which leaves four independent Mn atoms in the same plane (see schematic in Fig. 10). As above we will keep the calculations within the dipolar approximation. For example, the general dipole structure factor of the $Q+(010)$ peaks $\sigma\text{-}\sigma'$ channel is

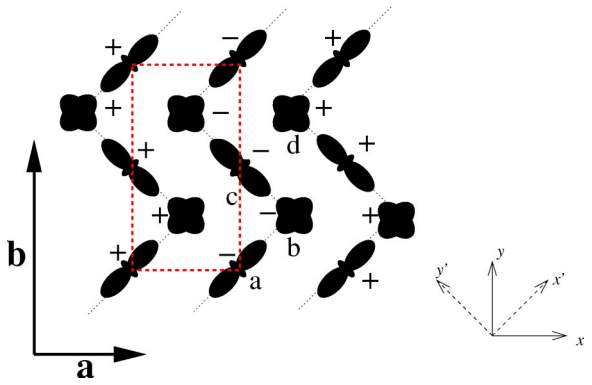

FIG. 10. Schematic diagram of the modified CE-type structure in the (**ab**) plane. The elongated figure-eights represent the occupied e_g $(3x'^2-r^2)$-type orbitals, while the clover shapes represent e_g $(x'^2-y'^2)$ orbitals. The signs + and − indicate the spin direction in the magnetically ordered phase. The letters denote the Mn for the model of the low-temperature phase only. The sites "*a*" and "*b*" correspond, respectively, to the sites 1 and 2 in the high-temperature phase. The dashed line indicates the unit cell.

$$F^{\mathrm{Mn}}_{\sigma\text{-}\sigma'}(0k0)=2[(f^{(a)}_{xx}-f^{(b)}_{xx}+f^{(c)}_{xx}-f^{(d)}_{xx})\sin^2\psi + (f^{(a)}_{zz}-f^{(b)}_{zz}+f^{(c)}_{zz}-f^{(d)}_{zz})\cos^2\psi + (f^{(a)}_{xz}-f^{(b)}_{xz}+f^{(c)}_{xz}-f^{(d)}_{xz})\sin 2\psi], \quad (9)$$

where *a*, *b*, *c*, and *d* label the four Mn sites within the plane (Fig. 10). In contrast to the high-temperature phase, the $(0k0)$ reflections are no longer forbidden as a result of very small displacements of the atoms. Therefore a term almost constant in energy must be added to the total structure factor to take into account the Thomson scattering and the resonant corrections from other absorption edges from all the atoms, arising from the fact that this scattering no longer precisely cancels. However, since we are interested mainly in the resonant contribution of the Mn atoms, and in any case these corrections are small, we will ignore them in the following, except where explicitly stated. As noted above, no resonance is measured at $\psi=0°$, so one infers from Eq. (9) that $f^{(a)}_{zz}-f^{(b)}_{zz}+f^{(c)}_{zz}-f^{(d)}_{zz}$ is zero within the limits of our experiment, the energy resolution of the experiment being about 5 eV.[14] In contrast, the resonant effect at $\psi=90°$ indicates that $f^{(a)}_{xx}-f^{(b)}_{xx}+f^{(c)}_{xx}-f^{(d)}_{xx}$ is nonzero.

Similarly, the general dipole structure factor for the $Q+(0\frac{1}{2}0)$ peaks $\sigma\text{-}\pi'$ channel is

$$F^{\mathrm{Mn}}_{\sigma\text{-}\pi'}\left(0\tfrac{k}{2}0\right)=-(f^{(a)}_{xx}+if^{(b)}_{xx}-f^{(c)}_{xx}-if^{(d)}_{xx})\sin\theta_B\sin 2\psi - (f^{(a)}_{xz}+if^{(b)}_{xz}-f^{(c)}_{xz}-if^{(d)}_{xz})\sin\theta_B\cos 2\psi + 2(f^{(a)}_{xy}+if^{(b)}_{xy}-f^{(c)}_{xy}-if^{(d)}_{xy})\cos\theta_B\sin\psi + 2(f^{(a)}_{yz}+if^{(b)}_{yz}-f^{(c)}_{yz}-if^{(d)}_{yz})\cos\theta_B\cos\psi + (f^{(a)}_{zz}+if^{(b)}_{zz}-f^{(c)}_{zz}-if^{(d)}_{zz})\sin\theta_B\sin 2\psi. \quad (10)$$

Using expressions such as Eqs. (9) and (10) we can proceed, constrained by the experimental data, to develop a model for the low-temperature electronic order.

2. Model of the CE-type electronic configuration

By considering various models of the COO phase, with particular symmetries between the Mn atoms one can simplify Eq. (9). The simplest model of the COO phase, as considered by García *et al.*,[22] is a checkerboard model in which Mn_b and Mn_d are identical and isotropic, i.e., $f^{(b)}_{xx}=f^{(b)}_{yy}=f^{(b)}_{zz}=f^{(d)}_{xx}=f^{(d)}_{yy}=f^{(d)}_{zz}=f$ and the off-diagonal terms are zero. For the sites *a* and *c*, they used an alternative notation, that is, $f^{(a)}_{xx}=f^{(c)}_{yy}=(f_{\parallel}+f_{\perp})/2$ and $f^{(a)}_{xy}=f_{\parallel}-f_{\perp}$ where $\parallel$ $(\perp)$ indicates the direction parallel (perpendicular) to the stretching of the e_g orbital.[22] This equivalent description will be convenient in a case described later for understanding the shape of the resonances. For our analysis, we make the less restrictive ansatz that the electron density of the Mn_b and Mn_d sites has a square symmetry in plane. At this point, this is a starting assumption. However, as we shall see, it is both consistent with our experimental data and recent theoretical calculations. Such in-plane symmetry can include, for example, the population of e_g orbitals of the $x'^2-y'^2$ or $3z'^2-r^2$ symmetry as suggested by recent theoretical calculations[16] [in labeling the orbitals we use the (x',y',z') coordinate system aligned along the extension of the e_g orbitals, see Fig. 10, to preserve the more familiar description of these orbitals]. In such a model, we force $f^{(b)}_{xx}=f^{(d)}_{xx}=f^{(b)}_{yy}=f^{(d)}_{yy}\neq f^{(b,d)}_{zz}$. Following the labels in Fig. 10, Mn_a and Mn_c have a $3x'^2-r^2$ and $3y'^2-r^2$ geometry, respectively. They are related by a $\pi/2$ rotation around the **c** axis (more accurately, they are related by a $\pi/2$ rotation about the principal axis of the octahedra which is tilted 10° from the **c** direction as a result of the tilt order), with the extension of the highest occupied $3d$ orbital and a concomittant extension of the Mn-O bonds along the $[110]$ and $[1\bar{1}0]$ directions. It follows that $f^{(c)}_{xx}=f^{(a)}_{yy}$, $f^{(c)}_{xz}=f^{(a)}_{xz}$, and $f^{(c)}_{xy}=-f^{(a)}_{xy}$. The resulting Mn structure factors in this model are

$$F^{\mathrm{Mn}}_{\sigma\text{-}\sigma'}\left(0\tfrac{k}{2}0\right)=2(f^{(a)}_{xx}-f^{(a)}_{yy})\sin^2\psi,$$

$$F^{\mathrm{Mn}}_{\sigma\text{-}\pi'}\left(0\tfrac{k}{2}0\right)=-(f^{(a)}_{xx}-f^{(a)}_{yy})\sin 2\psi\sin\theta_B + 4f^{(a)}_{xy}\sin\psi\cos\theta_B,$$

$$F^{\mathrm{Mn}}_{\sigma\text{-}\sigma'}(0k0)=2f^{(a)}_{xx}+f^{(a)}_{yy}-2f^{(b)}_{xx})\sin^2\psi+4(f^{(a)}_{zz}-f^{(b)}_{zz}) \times\cos^2\psi+4(f^{(a)}_{xz}-f^{(b)}_{xz})\sin 2\psi,$$

$$F^{\mathrm{Mn}}_{\sigma\text{-}\pi'}(0k0)=4f^{(b)}_{xy}\sin\psi\cos\theta_B+4(f^{(a)}_{yz}-f^{(b)}_{yz})\cos\psi\cos\theta_B - 2(f^{(a)}_{xz}-f^{(b)}_{xz})\cos 2\psi\sin\theta_B + \sin 2\psi\sin\theta_B[2(f^{(a)}_{zz}-f^{(b)}_{zz})+2f^{(b)}_{xx} - (f^{(a)}_{xx}+f^{(a)}_{yy})]. \quad (11)$$

Note again that for simplicity these relations neglect the fact that the Mn atoms are slightly displaced. This displacement will give rise to small corrections to the expressions. However, for the present purposes, we are concerned with which components will contribute to the resonant scattering and the associated azimuthal dependence, for which, these corrections are unimportant. Below, we write explicitly these scattering factors for two limits of azimuthal geometries, $\psi = 90°$ and $\psi = 0°$.

For $\psi = 90$,

$$F^{\mathrm{Mn}}_{\sigma\text{-}\sigma'}\left(0\frac{k}{2}0\right) = 2(f^{(a)}_{xx} - f^{(a)}_{yy}), \tag{12}$$

$$F^{\mathrm{Mn}}_{\sigma\text{-}\pi'}\left(0\frac{k}{2}0\right) = 4f^{(a)}_{xy}\cos\theta_B, \tag{13}$$

$$F^{\mathrm{Mn}}_{\sigma\text{-}\sigma'}(0k0) = 2[(f^{(a)}_{xx} + f^{(a)}_{yy}) - 2f^{(b)}_{xx}], \tag{14}$$

$$F^{\mathrm{Mn}}_{\sigma\text{-}\pi'}(0k0) = 4f^{(b)}_{xy}\cos\theta_B + 2(f^{(a)}_{xz} - f^{(b)}_{xz})\sin\theta_B. \tag{15}$$

For $\psi = 0$,

$$F^{\mathrm{Mn}}_{\sigma\text{-}\sigma'}\left(0\frac{k}{2}0\right) = 0, \quad F^{\mathrm{Mn}}_{\sigma\text{-}\pi'}\left(0\frac{k}{2}0\right) = 0, \tag{16}$$

$$F^{\mathrm{Mn}}_{\sigma\text{-}\sigma'}(0k0) = 4(f^{(a)}_{zz} - f^{(b)}_{zz}), \tag{17}$$

$$F^{\mathrm{Mn}}_{\sigma\text{-}\pi'}(0k0) = 4(f^{(a)}_{yz} - f^{(b)}_{yz})\cos\theta_B - 2(f^{(a)}_{xz} - f^{(b)}_{xz})\sin\theta_B. \tag{18}$$

3. On the $Q+(0\frac{1}{2}0)$ reflections

As can be seen from Eq. (13), only the off-diagonal component $f^{(a)}_{xy}$ is measured in the σ-π' channel at $\psi = 90°$. This is the same matrix element that the $(0k0)_{\sigma\text{-}\pi'}$ reflections are sensitive to at *high* temperatures [at low temperatures the $(0k0)_{\sigma\text{-}\pi'}$ reflections depend on the f_{xy} term of Mn_b, as the Mn_a and Mn_c f_{xy} terms cancel with each other]. One can in principle therefore follow the temperature dependence of the $f^{(a)}_{xy}$ term above and below the transition by tracking the temperature dependence of the $(0k0)_{\sigma\text{-}\pi'}$ and $(0\ k/2\ 0)_{\sigma\text{-}\pi'}$ peaks, respectively.

Focusing on the energy line shape, one observes a strong intensity for $I(0\frac{3}{2}0)_{\sigma\text{-}\pi'}$ at the absorption edge (Fig. 6). In particular, this energy dependence is strongly reminiscent of the resonant signal observed from the prototypical Jahn-Teller system $LaMnO_3$,[27] shown in Fig. 7. In the context of the present model, the similarity between the $LaMnO_3$ $(010)_{\sigma\text{-}\pi'}$ and the $Pr_{0.6}Ca_{0.4}MnO_3$ $(0\frac{3}{2}0)_{\sigma\text{-}\pi'}$ spectra is explained naturally by the fact that the Mn_a and Mn_c undergo a Jahn-Teller distortion as a result of the orbital ordering while the Mn_b and Mn_d maintain an in-plane square symmetry. At the $Q+(0\frac{1}{2}0)$ reflections, the Mn_b and Mn_d contributions cancel. We note that this similarity of the energy line shapes is not a trivial result—the $(010)_{\sigma\text{-}\pi'}$ line shape at high temperatures, which measures the same component of the tensor, appears quite different: It has a smaller first resonance and a larger second resonance (Figs. 4 and 6). Thus, the similarity of the resonances is a strong evidence that the distortions—and thus the occupied orbitals—are the same in the two cases. For $LaMnO_3$, the existence of $3x'^2 - r^2/3y'^2 - r^2$ orbital order is unquestioned and we conclude that it is the same orbital order involved here on the Mn_a and Mn_c sites.

However, we do not believe the $(3x'^2 - r^2)$- and $(3y'^2 - r^2)$-like orbitals are fully occupied. Indeed, as discussed below, we will conclude, from an analysis of the $Q+(010)$ reflections that the charge disproportionation is incomplete, and that there is a partial occupancy of the $x'^2 - y'^2$ orbitals on the Mn_b and Mn_d sites.

4. On the Q+(010) reflections

For $(0k0)_{\sigma\text{-}\sigma'}$, at $\psi = 90°$, one measures the in-plane anisotropy, i.e., $f^{(a)}_{xx} + f^{(a)}_{yy} - 2f^{(b)}_{xx}$ which is the difference between the sum $f^{(a)}_{xx} + f^{(c)}_{xx} = f^{(a)}_{xx} + f^{(a)}_{yy}$ for the sites Mn_a and Mn_c and the same sum for the sites Mn_b and Mn_d, that is, $f^{(b)}_{xx} + f^{(d)}_{xx} = 2f^{(b)}_{xx}$ [Eq. (14)]. The observation of a resonance (see Fig. 5) indicates that $f^{(a)}_{xx} + f^{(a)}_{yy} - 2f^{(b)}_{xx}$ is nonzero. This implies directly that the in-plane orbital occupancy is different on the two sites.

An important question is whether this difference in the resonant factors arises from a chemical shift of the $1s$ levels as expected for charge ordering. It is noteworthy that, as reported by Zimmermann *et al.*,[14] the resonant signal from $F^{\mathrm{Mn}}_{\sigma\text{-}\sigma'}(0k0)$ disappears at $\psi = 0°$. This indicates that $f^{(a,c)}_{zz} = f^{(b,d)}_{zz}$ [Eq. (18)]: thus there is no *measurable* difference in the out-of-plane configuration between the two sites. As noted previously by Nakamura *et al.*[6] and García *et al.*[22] it is difficult to understand the disappearance of the resonant signal at $\psi = 0°$, that is, the equality of the out-of-plane resonant factors, $f^{(a,c)}_{zz}$ and $f^{(b,d)}_{zz}$, if the resonance involves a chemical shift of the $1s$ levels, which would be expected to produce an isotropic effect on the resonant factor. We discuss in the following the case with and without a chemical shift of the $1s$ levels.

First, let us consider that there is a significant chemical shift of the $1s$ levels. Then one would be forced to conclude that the equality between $f^{(a,c)}_{zz}$ and $f^{(b,d)}_{zz}$ is accidental and due to a relatively small magnitude of the $1s$ chemical shift together with an out-of-plane population of the orbitals. This would give rise to small and different displacements along the **c** direction whose effect on the resonant factors would have to exactly counterbalance the $1s$ chemical shift. For example, the in-plane stretching of the e_g $(3x'^2 - r^2)$-type orbital on sites *a* and *c* brings the oxygens along the *z* direction closer to Mn_a and Mn_c thereby raising the resonance energy along the *z* direction. This brings the spectrum of $f^{(a,c)}_{zz}$ closer to $f^{(b,d)}_{zz}$. In addition, one could allow a population of the $3z'^2 - r^2$ orbital on the $\mathrm{Mn}_{b,d}$ atoms (as predicted theoretically by van den Brink *et al.*[16]). This would imply an increase of the out-of-plane distance Mn-O along **c** on the sites *b* and *d*, which would also lower the $4p$ orbitals along the **c** axis thereby shifting $f^{(b,d)}_{zz}$ closer to $f^{(a,c)}_{zz}$. However, this cancellation requires that the shift of the $1s$ and $4p$ be precisely the same to cancel each other. Further, in

$Nd_{0.5}Sr_{0.5}MnO_3$ one also observes no resonance at $\psi=90°$, thus requiring the same accidental cancellation to occur in two different materials.[6] Thus, a chemical shift of the $1s$ level appears unlikely.

Conversely, if one assumes there is no shift of the $1s$ level, then the resonant signal at $Q+(010)$ and $Q+(0\frac{1}{2}0)$ must arise from structural distortions associated with the orbital ordering. Indeed, as the spectra of the $Q+(0\frac{1}{2}0)$ reflections are similar to those of $LaMnO_3$, it seems likely that, as discussed above, the signal at these reflections comes mostly from the Jahn-Teller distortions, that is, an anisotropic energy shift of the $4p$ levels. Furthermore, we show in the following section that *ab initio* calculations of the RXD spectra, for the distorted structure, reproduce the line shape of both the $Q+(0\frac{1}{2}0)$ and $Q+(010)$ reflections suggesting that they have a common origin (the two types of reflections have different energy line shape in part because for the latter reflections there is interference with the nonresonant Thomson scattering in the σ-σ' channel).

The different in-plane configuration explains the resonant signal when the polarization points in the plane ($\psi=90°$) and the absence of any difference for the out-of-plane configuration explains the absence of a resonant signal when $\psi=0°$. It is likely that the mean Mn-O distance is therefore the same along **c** for all sites.

Finally, our results explain the azimuthal dependence of the intensity at an $(0k0)_{\sigma\text{-}\sigma'}$ reflection as arising mainly due to the term $f_{xx}^{(a)}+f_{yy}^{(a)}-2f_{xx}^{(b)}$ (here we have also used the expectation that the off-diagonal term $f_{xz}^{(a,c)}-f_{xz}^{(b,d)}$ is negligible compared to the diagonal terms). The intensity depends on the ratio of the resonant contribution and the Thomson terms. At resonance, the signal is about four times that of the Thomson scattering as deduced from the off-resonant intensity. So the contributions from Thomson scattering and resonant scattering of the Mn atoms are of a similar amplitude. In this case, it is easily shown that the azimuthal dependence of the σ-σ component is $1+2\sin^2\psi+\sin^4\psi$ (again ignoring the off-diagonal terms). Indeed, a twofold dependence has been measured for these reflections.[14]

High-resolution XANES studies have not shown a difference between the scattering factors of the two different Mn sites at low temperature.[20] Conversely, as we have just shown, the RXD measurements demonstrate that there are two differentiable Mn sites with two different scattering factors. The limitation in using the XANES technique for studies of small electronic reorganizations arises from the fact that it measures the sum of the contributions from all sites. The different spectra are thus smeared out. This limitation is worsened if the XANES measurements are performed on powder samples because the spectrum is then the average over all directions for which there are different absorption edges. Even on single crystals the differences in scattering power are difficult to observe because of the presence of twinning. [We observed three domains in our sample: an **a** domain, a **b** domain, and another domain propagating along the (112) direction.] Thus, XANES measurements are inherently insensitive to small energy shifts of the resonant factors. In contrast, RXD can directly measure the difference in the scattering factors. Moreover the direction of the polarization is well defined with respect to the crystallographic axes when measuring a Bragg reflection of a specific domain and twinning does not present a problem. In the present case, the sensitivity appears as the so-called derivative effect for the $Q+(010)$ and $Q+(100)$ reflections with the azimuthal angle $\psi=90°$, that is, the polarization is directed along the **a** and **b** crystallographic directions, respectively. The XANES measurements do confirm that the chemical shift must be smaller than 4.5 eV, the value obtained by comparing the parent compounds. Such a large difference would be detected by XANES. Thus, XANES does not support a complete charge disproportionation, in which one assumes that the oxygen octahedra for the formal $3+$ and $4+$ Mn atoms in $Pr_{0.6}Ca_{0.4}MnO_3$ are the same as in $LaMnO_3$ and $CaMnO_3$ structures, respectively.[20] The XANES measurements are, however, not inconsistent with a small disproportionation.[20]

To summarize, there is no evidence of a $1s$ chemical shift that might arise from charge disproportionation, and the electronic configuration may be regarded as an orbital ordering of the Mn on inequivalent sites arranged in a checkerboard pattern. The resonant effect arises mainly due to a $4p$ shift induced by the cooperative Mn-O distance modulations resulting from the orbital ordering. We observe a Jahn-Teller (JT) distortion on half of the Mn atoms. That is, half the Mn atoms have an in-plane symmetry [$(3x^2-r^2)$-like] and half are symmetric in plane. However, since there is no strong evidence of charge disproportionation, we suggest that the other half of the sites have a partially occupied $x'^2-y'^2$ orbital. To be more specific, one might write the electron configuration of neighboring Mn atoms A and B as $|A;B\rangle=\alpha|3d^4,3z^2-r^2;3d^3\rangle+\beta|3d^3;3d^4,x^2-y^2\rangle$, where $|3d^4,3z^2-r^2;3d^3\rangle$ refers to a configuration on Mn A with four electrons in the d band, the fourth electron in a $(3z^2-r^2)$-like orbital, and with the neighbor Mn in a $3d^3$ configuration.[47] When $\alpha=\beta=1/\sqrt{2}$ there is orbital ordering without charge ordering. Any occupancy of the $3z'^2-r^2$ orbital must occur either equivalently on all sites or with a random distribution, that is, the data exclude any ordered difference along the **c** direction between the two sites.

Finally, we comment on the charge disproportionation. While there is no direct evidence for significant disproportionation—in the form of a chemical shift of the $1s$ levels—the charge on the two Mn sites, as defined as the charge contained within a sphere of given size, is unlikely to be the same on the JT distorted site as on the undistorted site because of the varying bond lengths. Thus the charge disproportionation is likely to be of the form $Mn^{\nu-\delta}$ and $Mn^{\nu+\delta}$ where ν is the average formal valence and $\delta<0.5$. From the existing data set we cannot set a lower limit on δ.

In the following section we show that the *ab initio* calculations of the RXD spectra support the existence of a checkerboard pattern of JT-distorted and regular oxygen octahedra.

5. Ab initio calculations with candidate crystallographic structures for half-doped manganites

We performed *ab initio* calculations of the XANES and RXD spectra for two crystallographic structures recently pro-

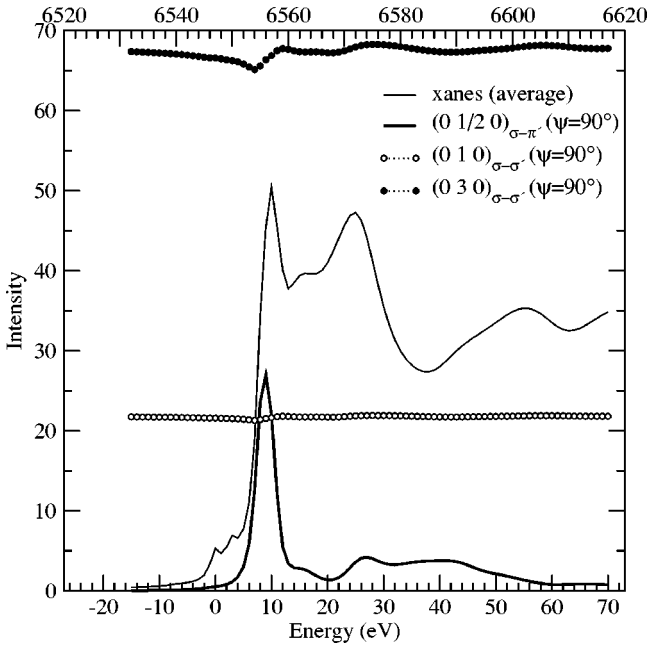

FIG. 11. *Ab initio* calculations of the XANES, $(0\frac{1}{2}0)_{\sigma\text{-}\pi'}$, $(010)_{\sigma\text{-}\sigma'}$, and $(030)_{\sigma\text{-}\sigma'}$ spectra using the $Pr_{0.6}Ca_{0.4}MnO_3$ crystallographic structure from Ref. 21. The spectra are calculated with the same scattering geometry as the data presented in Figs. 5 and 6.

posed for the low-temperature phase of the half-doped manganites, the so-called ''charge and orbital ordered'' phase. The FDMNES code and the same procedure described in the Sec. IV A were used. First, we used the refinement of Daoud-Aladine *et al.*[21] for $Pr_{0.6}Ca_{0.4}MnO_3$ which is inconsistent with the checkerboard model. Second, we used the structure of Radaelli *et al.* for $La_{0.5}Ca_{0.5}MnO_3$,[5] which reports a checkerboard model of inequivalent Mn atoms. We did not use the refinement of Lees *et al.*[46] for $Pr_{0.6}Ca_{0.4}MnO_3$ which shows a checkerboard pattern of inequivalent Mn, because in this structure the $Q+(010)$ reflections have zero nonresonant intensity in contradiction with the data.

The results for the structure proposed by Daoud-Aladine *et al.*,[21] the so-called Zener-polaron model, are shown in Fig. 11. For the $(010)_{\sigma\text{-}\sigma'}$ and $(030)_{\sigma\text{-}\sigma'}$ reflections, the resonant contribution is at least one order of magnitude smaller than the Thomson contributions of the other atoms. The structure fails to reproduce the strong resonant signal. We can understand the absence of a resonant effect in these calculations as follows. The proposed space group is $P11m$ (monoclinic), with a strong orthorhombic $P2_1nm$ pseudosymmetry. The Mn_a and Mn_b atoms are then situated at equivalent crystallographic sites and have the same valence and orbital geometry. Instead, the inequivalent sites in the $P2_1nm$ space group are the ''*A*'' sites (in our notation, the Mn_a and Mn_b sites) and the ''*C*'' sites (Mn_c and Mn_d). Such a structure is inconsistent with the checkerboard-type model and is the basis for introducing a Zener-polaron model. The total structure factor for the Mn atoms in this model is

$$F^{\mathrm{Mn}}(h00) \approx F^{\mathrm{Mn}}(0k0) \approx -4(f_{xy}^{A} - f_{xy}^{C}) \begin{pmatrix} 0 & 1 & 0 \\ 1 & 0 & 0 \\ 0 & 0 & 0 \end{pmatrix}, \quad (19)$$

with h and k odd. The approximation made here is that $e^{i2\pi k\varepsilon} \approx 1$, where ε describes the small relative displacement of the Mn atoms in the low-temperature unit cell, ε is typically of the order of 1/1000.[21] For the $F(h00)$ reflections, the diagonal terms cancel exactly, and the model gives no resonant contribution in the σ-σ' channel at any azimuthal orientation (these reflections are indeed forbidden in the $P2_1nm$ space group). For the $F(0k0)$ reflections, the diagonal terms do not cancel exactly due to the small relative displacements between equivalent atoms. However, the structure factor calculated from the refined atomic positions shows that the cancellation is still almost complete and the resonance is damped.

Here, the empirical observation of a strong resonant effect for $(0k0)$ reflections requires that Mn_a and Mn_b are in different crystallographic sites and that they are surrounded by different oxygen octahedra. This deduction is independent of any debate over the origin of the anisotropy; it is simply a statement about the different anisotropies of the two sites and implies that they cannot be related by a mirror, a translation, or a π rotation. In the $P11m$ space group the positions of the atoms are said to be almost the same as those in the $P2_1nm$ space group,[21] that is, Eq. (19) certainly still holds. Allowing significant differences in the atomic positions would change Eq. (19) but it would also no longer represent the Zener-polaron model. By going toward a checkerboard model of inequivalent sites, one explains the large spectroscopic effects observed experimentally.

Also, as shown in Fig. 12, high-resolution measurements of the $(0k0)$ reflections reveal an apparent splitting in reciprocal space. We attribute this splitting to the presence of $(h00)$ and $(0k0)$ reflections from perpendicular (twin) domains. However $Q+(100)$ reflections are forbidden in the $P2_1nm$ space group, and although the monoclinic $P11m$ permits the appearance of intensity at $Q+(100)$ positions, in the candidate structure they are expected to be much smaller than at $Q+(010)$ positions because of the pseudosymmetry found with almost the same positions.[21] In fact, we observe similar intensities for these two types of reflections, together with a similar, but not identical, energy dependence. The observed splitting corresponds to two lattice parameters, assumed to be **a** and **b**, differing by $\Delta = 0.013$ Å. This is consistent with measurements of the in-plane lattice parameters (a and b) in the COO phase: $a = 5.4315$ Å, $b = 2\times 5.4485$ Å and $c = 7.6370$ Å, so $\Delta = 0.017$ Å. Similarly Lees *et al.* reported $a = 5.4313$ Å, $b = 2\times 5.4413$ Å, and $c = 7.6022$ Å, that is, $\Delta = 0.01$ Å at 200 K. So it seems very likely that they are in fact **a** and **b** twin domains.

In Fig. 13 we show the energy dependence for the two peaks measured in the vicinity of (030) at $T = 100$ K. The (300) and (030) reflections have similar intensity in the energy-dependent spectra, which suggests that the displacements of the Mn atoms along **a** and **b** are similar. The difference between the spectra at 6576 eV presumably comes from the different polarization directions along the **b** and **a** directions, respectively. Interestingly, although the maximum is exactly at the same energy position for both spectra (within the 1 eV/step resolution), other features (such as the pre-edge anomaly at 6541 eV) seem to be shifted by 1 eV. In

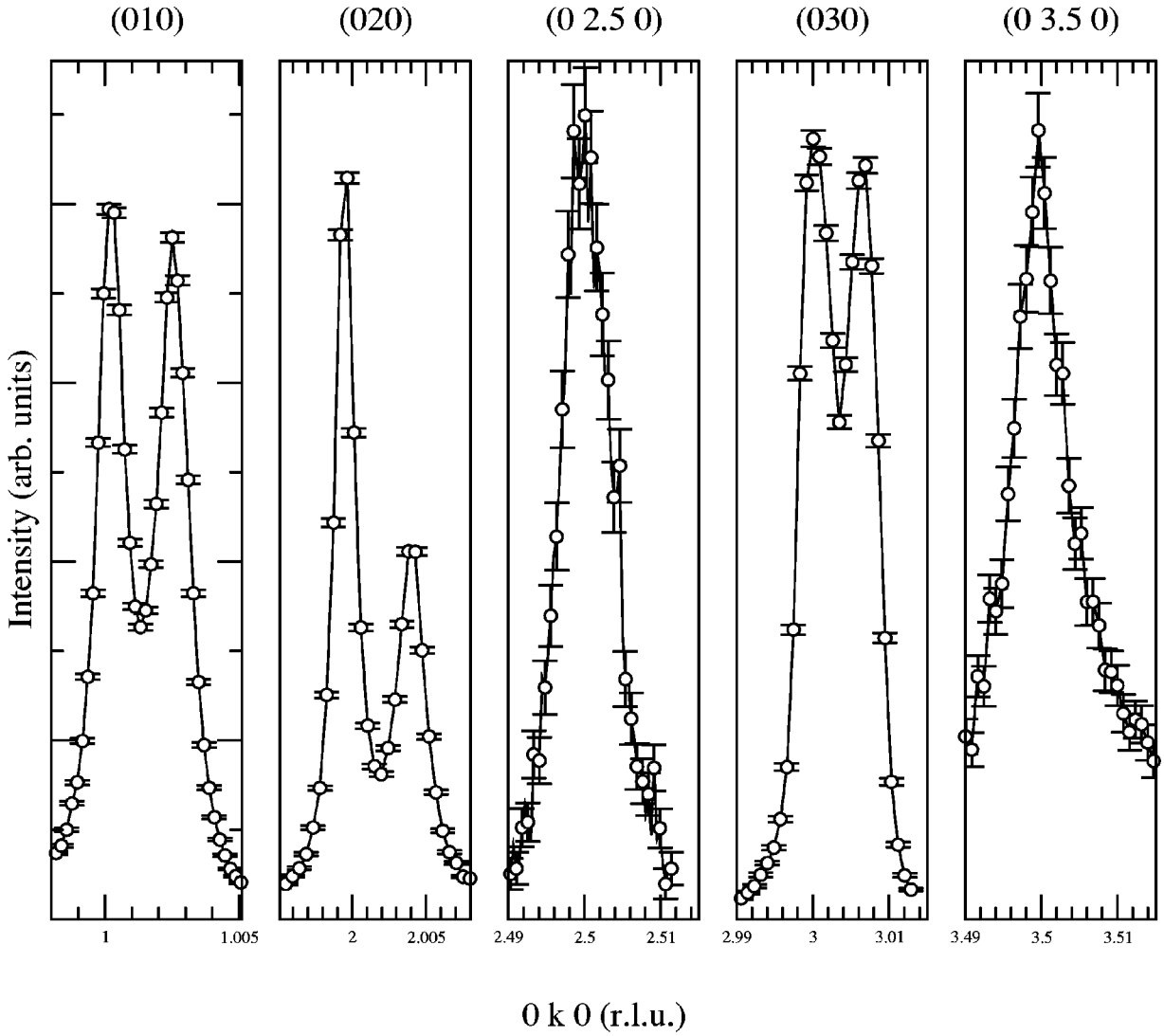

FIG. 12. Evidence of $(k00)$ and $(0k0)$ reflections, k odd, in the low-temperature phase (200 K). The reflections were measured with a high-resolution Ge(111) analyzer. The splitting observed at the $(0k0)$ reflections is attributed to $(0k0)$ and $(k00)$ reflections due to the presence of a nearby twinned domain; the separation corresponds to two lattice parameters differing by 0.013 Å consistent with the difference in **a** and **b** lattice parameters at this temperature. At the $(0\ k/2\ 0)$ reflections, there is no splitting as the doubling of the unit cell occurs only along the **b** axis. The data are not adjusted for differences in attenuation.

summary, it seems entirely plausible that these peaks originate from different crystallographic domains and that the actual structure gives equivalent $Q+(100)$ and $Q+(010)$ reflections. We note that the reflections $Q+(100)$ and $Q+(010)$ are present, with equivalent intensity, in the structure of the COO phase of $La_{0.5}Ca_{0.5}MnO_3$ as refined by Radaelli *et al.*[5]

We next show in Fig. 14 the results of *ab initio* calculations with the crystallographic structure of $La_{0.5}Ca_{0.5}MnO_3$ as refined by Radaelli *et al.*[5] The space group is $P2_1/m$ and the inequivalent Mn are organized in the checkerboard model, suggesting the CE-type ordering and consistent with the present picture for $Pr_{0.6}Ca_{0.4}MnO_3$. In this structure, half of the Mn atoms have a Jahn-Teller distortion, the other half are situated in regular, undistorted, octahedra. The calculations of the XANES, the $(0\frac{1}{2}0)_{\sigma\text{-}\pi'}$, $(010)_{\sigma\text{-}\sigma'}$, and $(030)_{\sigma\text{-}\sigma'}$, reflection spectra are in very good agreement with the data (Figs. 5 and 6). This structure also explains the observation of the $Q+(100)$ and $Q+(010)$ reflections. In Fig. 15 the calculated spectra for the (300) and (030) reflections are shown. The fine structures, above the absorption edge, are in good agreement with the data presented in Fig. 13, reproducing both the similarities and differences between the two reflections between 6560 eV and 6590 eV. Also, the pre-edge region below 6550 eV is well reproduced. The pre-edge feature marked by an arrow in Fig. 5 is identified as a dipole transition because only the dipolar operator is used in the calculations. However this feature appears 9.5 eV below the absorption edge (maximum of the first derivative) instead of 14 eV in the data. Presumably, this is in part because of the approximation that the Mn atom is charge neutral, $3d^5 4s^2$, thus details of the $3d$ band states will not be well reproduced. Further calculations based on the finite difference method beyond the muffin-tin approximation for the

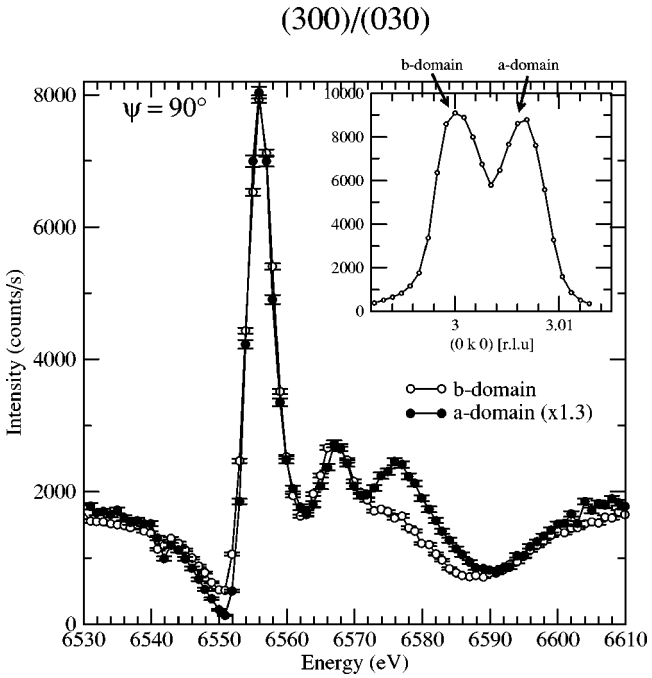

FIG. 13. Incident energy dependence of the two peaks observed at the (030) position at $T=100$ K shown in the inset. The peak at $k=3.00$ is attributed to the **b** domains, i.e., to the (030) reflection, while the one at $k=3.006$ to the **a** domains, i.e., to the (300) reflection. The two spectra are scaled for clarity.

atomic potentials are planed to improve the pre-edge spectra. Such study is beyond the scope of the present work.

These results suggest that the displacements of the atoms, in particular the oxygen atoms, are equivalent in $Pr_{0.6}Ca_{0.4}MnO_3$ to those observed in $La_{0.5}Ca_{0.5}MnO_3$. In particular, one notes that in the $La_{0.5}Ca_{0.5}MnO_3$ structure the Mn-O distances along the *c* direction are equivalent for all sites, explaining the absence of RXD signal when the polarization of the photons is along the *c* direction. In this $La_{0.5}Ca_{0.5}MnO_3$ structure there is no displacement of the Mn along the *b* direction, however a previous report[14] on the observation of a resonant signal on the $(0\ k/2\ 0)_{\sigma\text{-}\sigma'}$ reflections indicates that the Mn atoms are actually also displaced along *b* at the phase transition in $Pr_{0.6}Ca_{0.4}MnO_3$.

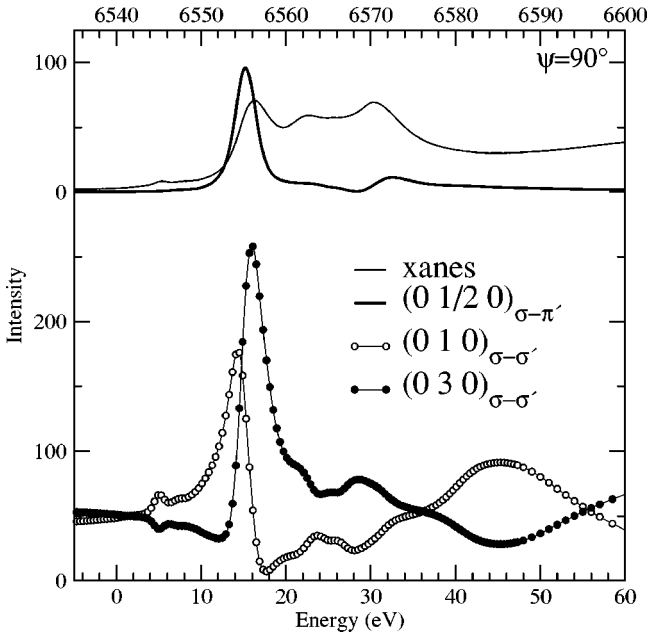

FIG. 14. *Ab initio* calculations of the XANES, $(0\,\frac{1}{2}\,0)_{\sigma\text{-}\pi'}$, $(010)_{\sigma\text{-}\sigma'}$, and $(030)_{\sigma\text{-}\sigma'}$ for the structure of $La_{0.5}Ca_{0.5}MnO_3$, in the so-called charge and orbital ordered phase, as refined by Radaelli *et al.* (Ref. 5). The results reproduce the data presented in Figs. 5 and 6. The curves are rescaled for clarity.

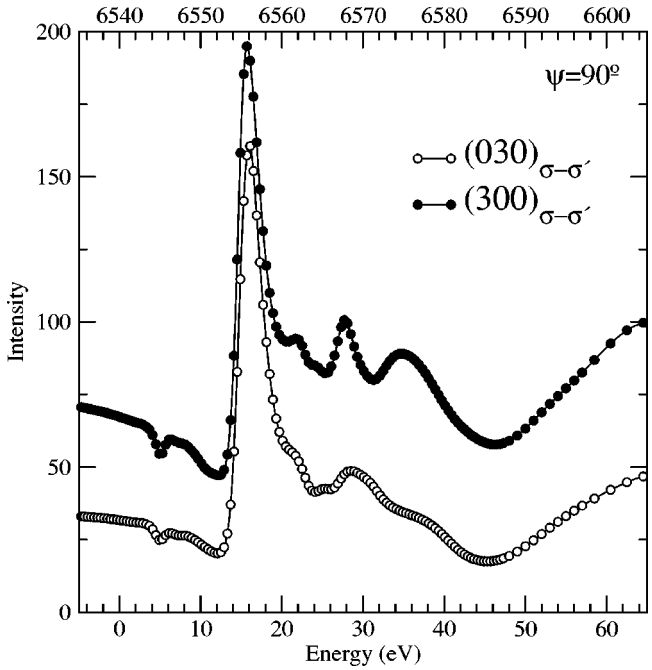

FIG. 15. *Ab initio* calculations of the $(300)_{\sigma\text{-}\sigma'}$ and $(030)_{\sigma\text{-}\sigma'}$ spectra with the structure of $La_{0.5}Ca_{0.5}MnO_3$ (Ref. 5). The results reproduce the data presented in Fig. 13.

In conclusion, the *ab initio* calculations of the RXD spectra strongly support a checkerboard pattern of inequivalent Mn atoms, in which half of the surrounding oxygen octahedra are Jahn-Teller distorted and the other half have a nearly square in-plane symmetry. Based on crystallographic and spectroscopic arguments, we find that the structure invoked for the Zener-polaron model cannot be correct. Instead, we determined that there must be a checkerboard pattern of the inequivalent Mn atoms with one electron localized on two Mn atoms.

V. SUMMARY

We have attempted to determine the pattern and the local geometry of the highest occupied orbital on the Mn sites in the near half-doped manganite $Pr_{0.6}Ca_{0.4}MnO_3$ using resonant x-ray scattering. We have emphasized that resonant diffraction cannot be considered as a definitive probe if only qualitative arguments are given, for example, the presence of a resonant signal in the σ-π channel and a particular azimuthal dependence. Rather, a careful analysis of the resonant spectra is required. This is especially true for the perovskite-

type reflections that mix charge, orbital, and tilt orderings of the oxygen octahedra.

Based on such considerations, we have presented a model for the low-temperature structure of $Pr_{0.6}Ca_{0.4}MnO_3$ which describes an orbitally ordered structure of the CE type. The CE structure is stabilized by a slight structural distortion which arises with the orbital ordering. Our experiments show that there is no measurable chemical shift of the Mn 1*s* levels. However it is likely that the orbital ordering implies a charge disproportionation from the mean valence v of the high-temperature phase (as defined as the charge contained around the two types of Mn sites). Therefore a charge disproportionation $Mn^{v-\delta}$ and $Mn^{v+\delta}$ with $\delta<0.5e^-$ might be considered. Unfortunately, at the present stage of the analysis, the RXD spectra—measured at the Mn *K* edge—do not permit us to set a lower limit on δ.

ACKNOWLEDGMENTS

We thank F. Bridges, A. Daoud-Aladine, J. García, J. Igarashi, Y. Joly, J. E. Lorenzo, P. G. Radaelli, and T. Vogt for fruitful discussions. We thank B. Ravel for the measurement of the absorption spectra on X11A at the NSLS. Use of the Advanced Photon Source was supported by the U.S. Department of Energy, Office of Science, Office of Basic Energy Sciences, under Contract No. W-31-109-Eng-38. Brookhaven National Laboratory is supported under DOE Contract No. DE-AC02-98CH10886. Support from the NSF MRSEC program, Grant No. DMR-0080008, is also acknowledged.

[1] *Physics of Manganites*, edited by T.A. Kaplan and S.D. Mahanti (Kluver, Academic, 1999).
[2] M.B. Salamon and M. Jaime, Rev. Mod. Phys. **73**, 583 (2001).
[3] Z. Jirák, S. Krupicka, Z. Simsa, M. Dlouhá, and S. Vratislav, J. Magn. Magn. Mater. **53**, 153 (1985).
[4] E. Wollan and W. Koehler, Phys. Rev. B **100**, 545 (1955).
[5] P.G. Radaelli, D.E. Cox, M. Marezio, and S.-W. Cheong, Phys. Rev. B **55**, 3015 (1997).
[6] K. Nakamura, T. Arima, A. Nakazawa, Y. Wakabashi, and Y. Murakami, Phys. Rev. B **60**, 2425 (1999).
[7] B.J. Sternlieb, J.P. Hill, U.C. Wildgruber, G. Luke, B. Nachumi, Y. Moritomo, and Y. Tokura, Phys. Rev. Lett. **76**, 2169 (1996).
[8] I.A. Zaliznyak, J.P. Hill, J.M. Tranquada, E. Erwin, and Y. Moritomo, Phys. Rev. Lett. **85**, 4353 (2000).
[9] R. Kajimoto, K. Ishizaka, H. Yoshizawa, and Y. Tokura, Phys. Rev. B **67**, 014511 (2003).
[10] E. Dagotto, T. Hotta, and A. Moreo, Phys. Rep. **344**, 1 (2001).
[11] J.B. Goodenough, Phys. Rev. **100**, 564 (1955).
[12] H. Kawano, R. Kajimoto, H. Yoshizawa, Y. Tomioka, H. Kuwahara, and Y. Tokura, Phys. Rev. Lett. **78**, 4253 (1997).
[13] J. Kanamori, J. Phys. Chem. Solids **10**, 87 (1959).
[14] M.v. Zimmermann, C.S. Nelson, J.P. Hill, D. Gibbs, M. Blume, D. Casa, B. Keimer, Y. Murakami, C.-C. Kao, C. Venkataraman, T. Gog, Y. Tomioka, and Y. Tokura, Phys. Rev. B **64**, 195133 (2001).
[15] V.I. Anisimov, I.S. Elfimov, M.A. Korotin, and K. Terakura, Phys. Rev. B **55**, 15 494 (1997).
[16] J. van den Brink, G. Khaliullin, and D. Khomskii, Phys. Rev. Lett. **83**, 5118 (1999).
[17] A.M. Oleś and L.F. Feiner, Phys. Rev. B **65**, 052414 (2002).
[18] P. Mahadevan, K. Terakura, and K. Sarma, Phys. Rev. Lett. **87**, 066404 (2001).
[19] Z. Popović and S. Satpathy, Phys. Rev. Lett. **88**, 197201 (2002).
[20] J. García, M.C. Sánchez, G. Subías, and J. Blasco, J. Phys.: Condens. Matter **13**, 3229 (2001).
[21] A. Daoud-Aladine, J. Rodríguez-Carvajal, L. Pinsard-Gaudart, M. Fernández-Díaz, and A. Revcoleschi, Phys. Rev. Lett. **89**, 097205 (2002).
[22] J. García, M.C. Sánchez, J. Blasco, G. Subías, and M.G. Proietti, J. Phys.: Condens. Matter **13**, 3243 (2001).
[23] Y. Tomioka, A. Asamitsu, H. Kuwahara, Y. Moritomo, and Y. Tokura, Phys. Rev. B **53**, 1689 (1996).
[24] Y. Okimoto, Y. Tomioka, Y. Onose, Y. Otsuka, and Y. Tokura, Phys. Rev. B **59**, 7401 (1999).
[25] Ch. Simon, S. Mercone, N. Guiblin, C. Martin, A. Brûlet, and G. André, Phys. Rev. Lett. **89**, 207202 (2002).
[26] D.H. Templeton, in *Resonant Anomalous X-Ray Scattering, Theory and Applications*, edited by G. Materlik, C.J. Sparks, and K. Fisher (Elsevier Science B.V., Amsterdam, 1994).
[27] Y. Murakami, J.P. Hill, D. Gibbs, M. Blume, I. Koyama, M. Tanaka, H. Kawata, H. Arima, Y. Tokura, K. Hirota, and Y. Endoh, Phys. Rev. Lett. **81**, 582 (1998).
[28] M. Benfatto, Y. Joly, and C.R. Natoli, Phys. Rev. Lett. **83**, 636 (1999).
[29] L. Paolasini, C. Vettier, F. de Bergevin, D. Mannix, A. Stunault, W. Neubeck, M. Altarelli, M. Fabrizio, P.A. Metcalf, and J.M. Honig, Phys. Rev. Lett. **82**, 4719 (1999).
[30] C. Vettier, J. Electron Spectrosc. Relat. Phenom. **117-118**, 113 (2001).
[31] D.H. Templeton and L.H. Templeton, Acta Crystallogr., Sect. A: Cryst. Phys., Diffr., Theor. Gen. Crystallogr. **36**, 237 (1980).
[32] P. Woodward, Acta Crystallogr., Sect. B: Struct. Sci. **53**, 44 (1997).
[33] M.v. Zimmermann, C.S. Nelson, Y.-J. Kim, J.P. Hill, D. Gibbs, H. Nakao, Y. Wakabayashi, Y. Murakami, Y. Tomioka, Y. Tokura, C.-C. Arima, T. Kao, D. Casa, C. Venkataraman, and T. Gog, Phys. Rev. B **64**, 064411 (2001).
[34] M. Takahashi, J.-I. Igarashi, and P. Fulde, J. Phys. Soc. Jpn. **68**, 2530 (1999).
[35] V.E. Dmitrienko, Acta Crystallogr., Sect. A: Found. Crystallogr. **39**, 29 (1983).
[36] M. Noguchi, A. Nakazawa, S. Oka, T. Arima, Y. Takabayashi, H. Nakao, and Y. Murakami, Phys. Rev. B **62**, 9271 (2000).
[37] M. Kubota, H. Nakao, Y. Murakami, J. P. Hill, D. Gibbs, Y. Tagushi, M. Iwama, and Y. Tokura (unpublished).
[38] M. Takahashi and J.-I. Igarashi, Phys. Rev. B **64**, 075110 (2001).
[39] M. Takahashi and J.-I. Igarashi, Phys. Rev. B **65**, 205114 (2002).
[40] J. Rodríguez-Carvajal, M. Hennion, F. Moussa, A.H. Moudden, L. Pinsard, and A. Revcolevschi, Phys. Rev. B **57**, 3189 (1998).

[41] I.S. Elfimov, V.I. Anisimov, and G.A. Sawatzky, Phys. Rev. Lett. **82**, 4264 (1999).
[42] Y. Joly, Phys. Rev. B **63**, 125120 (2001).
[43] S. Grenier, A. Toader, J.E. Lorenzo, Y. Joly, B. Grenier, S. Ravy, L.P. Regnault, H. Renevier, J.Y. Henry, J. Jegoudez, and A. Revcolevschi, Phys. Rev. B **65**, 180101 (2002).
[44] Y. Murakami, H. Kawada, M. Tanaka, T. Arima, Y. Moritomo, and Y. Tokura, Phys. Rev. Lett. **80**, 1932 (1998).
[45] U. Staub, G.I. Meijer, R. Allenspach, J.G. Bednorz, J. Karpinski, S.M. Kazakov, L. Paolasini, and F. d'Acapito, Phys. Rev. Lett. **88**, 126402 (2002).
[46] M. Lees, J. Barratt, G. Balakrishnan, D. Mc Paul, and C. Ritter, Phys. Rev. B **58**, 8694 (1998).
[47] K.J. Thomas, J.P. Hill, Y.-J. Kim, S. Grenier, P. Abbamonte, L. Venema, A. Rusydi, Y. Tomioka, Y. Tokura, D.F. McMorrow, and M. van Veenendal, cond-mat/0311553 (unpublished).